Aerodynamic simulation of heat shield separation test on ground

D. Chakraborty
Aerodynamics Division
Vikram Sarabhai Space Center, Kerala, India

S. Vasantha
SHAR Center
Shriharikota, India

ABSTRACT

The ability of a CFD technique to evaluate the performance of a heat shield separation system has been demonstrated. The evolution of the differential pressure across the heat shield surface has been estimated. The results of the analysis have been compared with the data from the separation test of the heat shield of an Indian launch vehicle. The pressure on the heat shield surface was estimated by solving the Navier Stokes equations using the Eulerian Lagrangian formulation. The results, which show good agreement with the observed results of a heat shield separation test on the ground, were found to be adequate for design purposes.

NOMENCLATURE

D	velocity divergence
f_r	body force component in radial direction
f_x	body force component in axial direction
I	internal energy
p	pressure
R	radius of heat shield fairing
t	time
u	velocity component in axial direction
v	velocity component in radial direction
x, y	coordinate directions
ρ	density
λ, μ	coefficients of viscosity
$\Pi_{xx}, \Pi_{yy}, \Pi_{xy}\ \Pi_\theta$	stress deviators

1.0 INTRODUCTION

The payload fairing in a rocket protects the satellite from aerodynamic loading, heating, acoustic vibrations and other adverse environmental conditions during launch and the ascent flight. The fairings are separated as soon as the vehicle gets outside the atmosphere. Convincing demonstration of jettisoning of the heat shield fairing — clean separation of the fairing halves, devoid of any possibility of re-contact with the vehicle or parts of the payload — is an imperative step in the development of any launch vehicle. During flight, the separation event occurs in near vacuum condition. The stringent requirements on the dynamic clearance of modern day fairings coupled with the need to keep the weight low, call for design of highly flexible fairing halves which undergo considerable deflection during separation. While this flexibility and consequent large deflection helps in attainment of large dynamic clearances during separation, it also makes the structural behaviour of the fairing half to become highly sensitive to minor changes in loading on the heat shield surface as, for example, may happen if the test were conducted in air instead of vacuum. Though the conduct of such a separation test on full scale model necessitates the availability of a large vacuum chamber and considerable expenditure, the importance of performing a reliable demonstration of the event has prompted the designers of rocket vehicles to persist in performing the test under vacuum conditions. For example the separation test of the flight standard version of Ariane 4 payload fairing (4m diameter and 9·6m height) was conducted in the Dynamic Test Chamber at ESTEC, Netherlands, stated to be the largest vacuum chamber in Europe. A detailed description of this test is available in Ref. 1. Similarly the separation tests on the payload fairings of the Atlas launch vehicle[2] were conducted in the world's largest vacuum chamber, at the Space Power Facility, Plum Brook, after simulating the altitude of jettison event.

In contrast with the usual method of qualification employed in the case of Ariane and Atlas heat-shields, the test on the heat shield of the Indian Polar Satellite Launch Vehicle (PSLV) was performed in air and the effects of the air were accounted for by analysis. The present study is an excellent example of the application of CFD capabilities for the solution of a practical problem of interest. A similar approach, though complete details are not available, also appears to have been adopted by the designers of the Japanese H-II rocket[3]. While the report does mention the measurement of the pressure inside the heat shield compartment, it is not clear whether any attempt was made to predict the heat shield response on the basis of analysis only or whether the experimental pressure data were used as the sole inputs for verifying the response. Present results have generated a sufficient degree of confidence to enable the designer to extrapolate the results of experiments in air to vacuum conditions. Heat shield separation system of PSLV was designed without conducting any test in a vacuum chamber, leading to large cost savings. Successful separation of heat shield fairings of all PSLV missions demonstrated the correctness of the approach.

Paper No. 2427. Manuscript received 16 June 1998, revised version received 5 June 1999, accepted 13 July 1999.

2.0 SEPARATION TEST

2.1 The experimental set up

Figure 1 shows a sketch of the PSLV heat shield separation test set up. The test article consists of a flight quality PSLV heat shield mounted on a simulated lower stage interface. The heat shield of aluminum isogrid construction consists of a conical upper section with spherical nose, a cylindrical middle section and a lower boat-tail section which mates with the top of the third stage of the launch vehicle. The shield is made of two half fairings joined along the longitudinal seam by the help of piston cylinder assembly with rubber bellows between the two. The cone-cylinder-boat-tail assembly is attached to the lower stage through a mermen band clamp. Up to the time of deployment, the heat shield fairing halves are held together — the piston being held in place within the cylinder — by shear rivets. The explosive cords are inside the bellows, kept within the cavity of the assembly. The bellows are bonded to the cylinder to prevent their detachment during the separation process. Two bellow systems are placed at the two diametrically opposite edges of the fairings. These are invariably interconnected at the top to provide redundancy. The jettisoning of the heat shield is achieved in two steps. The first consists in activating a horizontal separation system which detaches it from the parent vehicle. This is followed by lateral separation system which throws the fairing halves apart. A single command simultaneously activates the pyrotechnic bolt cutter releasing the mermen band and the ignition of the explosive in the zip cord. Ignition of explosive in the zip chord causes the bellow pressure to increase enormously, resulting in the shearing of the rivets and the impulsive ejection of the two halves of the fairing.

Two tests were conducted. The first one took place before the effects of the air on separation were clearly understood and the second one was repeated with additional instrumentation consisting of:

1. Pressure transducers to record the pressure inside the heat shield compartment and on the surface.
2. Strain gauges mounted on the surface.
3. Accelerometers on the heat-shield surface.
4. Measurement of bellow pressure to compute delivered impulse.
5. Optical sensors to determine the time when bellow is losing contact with the piston.

The locations of the pressure transducers (cp_1 to cp_{12}) are shown in Fig. 1. The achievement of minimum separation distance was confirmed by the use of snap gauges. A detailed description of the experiments conducted and the data generated has been presented in Ref. 4.

3.0 ANALYSIS

In this paper we have evaluated the transient behaviour of the compartmental pressure by solving the two-dimensional Navier Stokes equations. A Simplified Arbitrary Lagrangian Eulerian (SALE) algorithm developed by Amsden, Hirt and Cook[5, 6] has been used to solve the equations after necessary modifications. The most important feature of this algorithm is that it uses both Eulerian and Lagrangian procedures to solve the governing equations and is applicable to flows at all speeds. The procedure uses a finite difference

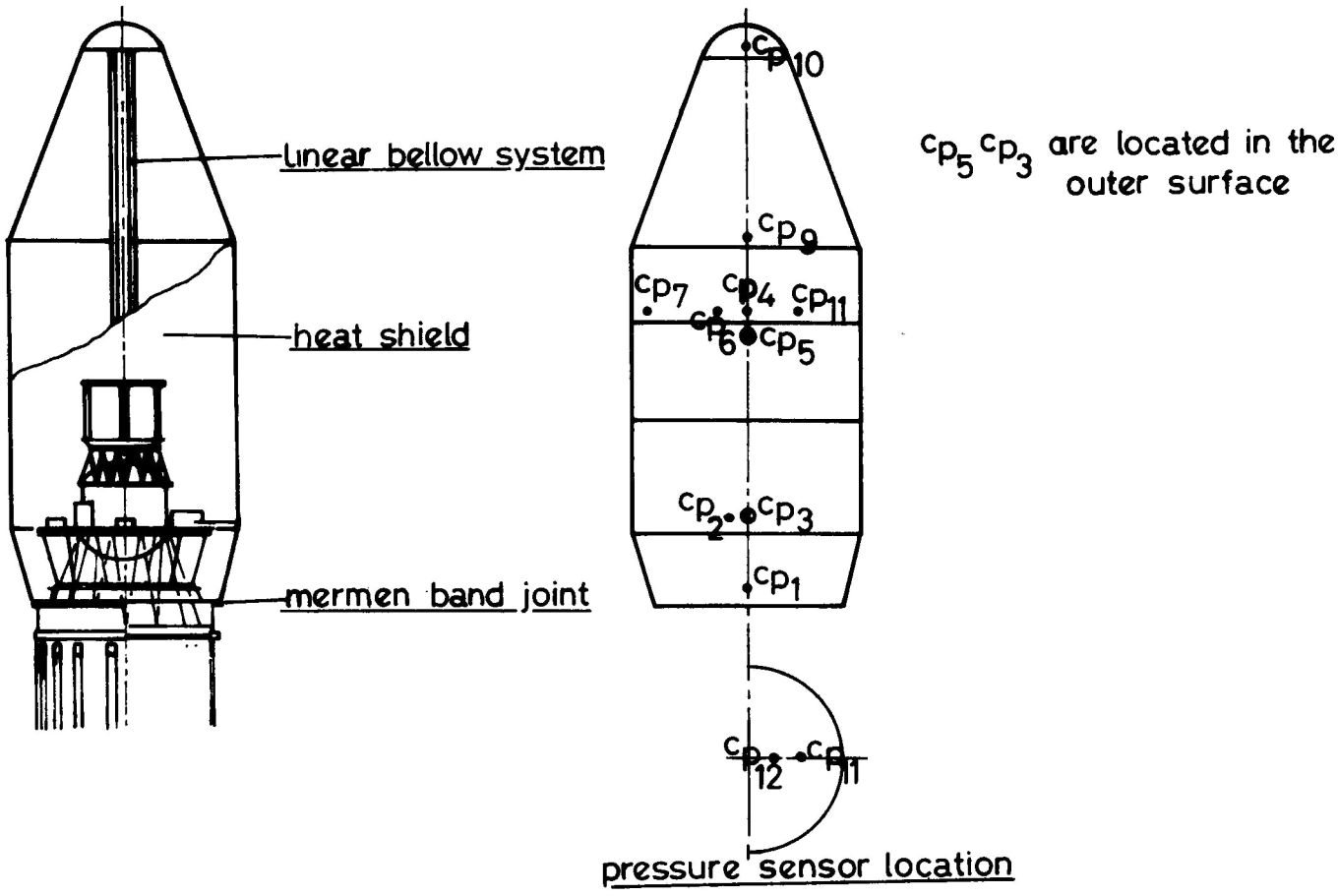

Figure 1. Set up for separation test of hield shield.

mesh with the vertices that may move with the fluid (Lagrangian), be held fixed (Eulerian) or be moved in any other prescribed way. The flow variables, pressure (p), density (ρ) and internal energy (I) are all assigned to cell centres, while the coordinates (x, y) and velocity components (u, v) are assigned to the cell vertices. The calculations necessary to advance the solution for one time step are performed in three distinct phases. In the first phase, explicit Lagrangian calculations are made, where convective fluxes are zero. In the second phase, which is optional, implicit calculations are made to obtain time advanced pressure forces. The main advantage of the second phase is that it eliminates the numerical stability condition that limits a sound wave to travel no further than one cell per time step. The cell vertices are moved to their new Lagrangian position after this phase. Finally in the third phase, which is also optional, the mesh can be relocated in a new position. In this re-zone phase, convective fluxes are computed to account for the movement of the fluid between cells as the mesh moves. Further details of the SALE algorithm are available in Ref. 6. In the present work, we have used the explicit Eulerian calculation only.

3.1 Governing equations

The Navier Stokes Equations in the axisymmetric form can be written as

Mass equation:

$$\frac{\partial \rho}{\partial t}+\frac{1}{r}\frac{\partial r\rho u}{\partial x}+\frac{\partial \rho v}{\partial y}=0 \qquad \ldots(1)$$

Axial momentum equation:

$$\frac{\partial \rho u}{\partial t}+\frac{1}{r}\frac{\partial r\rho u^2}{\partial x}+\frac{\partial \rho uv}{\partial y}=\frac{\partial p}{\partial y}+\frac{1}{r}\frac{\partial r\Pi_{xx}}{\partial x}+\frac{\partial \Pi_{xy}}{\partial y}+\frac{\Pi_\theta}{r}+\rho f_\infty \qquad \ldots(2)$$

Radial momentum equation:

$$\frac{\partial \rho v}{\partial t}+\frac{1}{r}\frac{\partial r\rho uv}{\partial x}+\frac{\partial \rho v^2}{\partial y}=\frac{\partial p}{\partial y}+\frac{1}{r}\frac{\partial r\Pi_{xy}}{\partial x}+\frac{\partial \Pi_{yy}}{\partial y}+\rho f_r \qquad \ldots(3)$$

Energy equation:

$$\frac{\partial \rho I}{\partial t}+\frac{1}{r}\frac{\partial r\rho Iu}{\partial x}+\frac{\partial \rho Iv}{\partial y}=-pD+\Pi_{xx}\frac{\partial u}{\partial x}+\Pi_{xy}\frac{\partial u}{\partial y}+\frac{u\Pi_\theta}{r}+\Pi_{xy}\frac{\partial v}{\partial x}+\Pi_{yy}\frac{\partial v}{\partial y} \qquad \ldots(4)$$

where D is the velocity divergence:

$$D=\frac{1}{r}\frac{\partial ru}{\partial x}+\frac{\partial v}{\partial y} \qquad \ldots(5)$$

Velocity components (u, v) are either in the Cartesian coordinates (x, y) or in the cylindrical coordinate (r, z). When Cartesian coordinates are desired, all radii r which appear in these equations are set to unity. The fluid pressure (p) is determined from the equation of state

$$p=p(\rho,I) \qquad \ldots(6)$$

The stress deviators are defined according to

$$\Pi_{xx}=2\mu\frac{\partial u}{\partial x}+\lambda D$$

$$\Pi_{yy}=2\mu\frac{\partial v}{\partial y}+\lambda D$$

$$\Pi_\theta=CYL\left(2\mu\frac{u}{r}+\lambda D\right) \qquad \ldots(7)$$

$$\Pi_{xy}=\mu\left(\frac{\partial u}{\partial y}+\frac{\partial v}{\partial x}\right)$$

where λ and μ are the coefficients of viscosity connected by the Stokes law, *viz*

$$3\lambda+2\mu=0 \qquad \ldots(8)$$

The coefficient *CYL* is zero for Cartesian coordinates and unity for cylindrical coordinates.

3.2 Idealisation of the problem

The firing of the explosive cord generates enormous lateral force projecting the fairing halves away from each other with a very large acceleration. Figure 2 depicts a typical recording of accelerometer data obtained during the test on the heat shield. This sudden motion in the presence of air gives rise to flow phenomena akin to the flow on the two sides of the diaphragm in a shock tube. The pressure differential between the two sides of the heat shield plays the primary role in diminishing the velocity gained and also in modifying the structural response of the heat shield to the impulsive forces acting on its edges. During this period the flow field is dominated by the waves generated by the sudden motion of the heat shield surface and their reflections.

For the purpose of estimating the compartmental pressure, the heat shield configuration (Fig. 1) is idealised as consisting of two concentric, infinitely long circular cylinders separating across a diametrical plane. We are thus ignoring the effect of the closed nose cone, the edge effects at the top and bottom extremities and also the presence of a number of components inside the heat shield which will modify the reflection of the waves. The radius of the inner cylinder corresponds to the radius of the spacecraft and the radius of the outer cylinder corresponds to the radius of the heat shield fairing. It is intuitively recognised that the pressure differential observed in the experiment will be higher than our estimates at the top and lower than the estimate at the bottom. The resulting occurrence of a nose closing tendency in the early phase of heat shield separation was indeed noted in the experiment.

By taking advantage of the symmetry condition, the computation is performed only for the upper half of the semi-circle.

3.3 Modelling of zipcord acceleration and atmospheric drag

During the first few milliseconds, when the zipcord system is in contact with the heat shield, the acceleration of the fairing is mainly dominated by the expansion of the bellow. The acceleration is found to reach its peak almost instantaneously with the initiation of the separation command and fall equally rapidly to zero when the contact with the bellow is lost. In the following period, the fairing is subjected to atmospheric drag due to the pressure differential between the outer

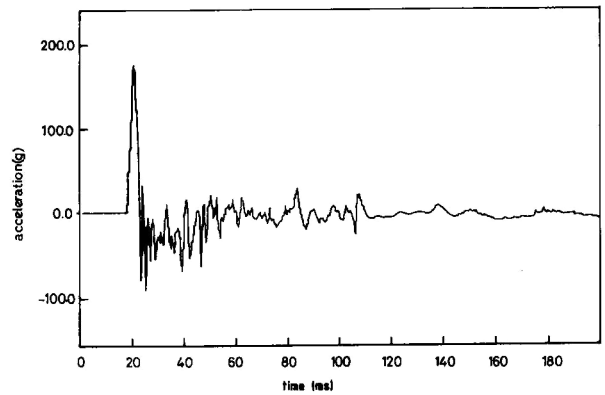

Figure 2. Typical acceleration profile.

surface and the inner surface. A linear model is employed in the simulation for the zipcord acceleration, and the atmospheric drag has been calculated at every time step from the computed pressure differential between the outer and inner surface of the heat shield fairing.

3.4 Computational grid

The grid network for the computational domain is shown in Fig. 3. The bottom boundary (AB) corresponds to the surface of the inner body (payload) inside the heat shield compartment and it is aligned with one mesh line. The heat shield surface is also aligned with a mesh line (EE) along the radial direction. The outer computational boundary (CD) is placed at a distance of five heat shield diameters beyond the heat shield fairing surface. The left boundary (AD) is placed in the plane of separation and in the plane of symmetry the center line boundary (BC) is placed.

A 38 × 40 grid is taken for the computation. In order to capture the complexity of the flow field, the mesh is relatively fine near the line of separation and the grid is exponentially stretched in the circumferential direction. In the radial direction, a uniform grid is employed in the gap between inner body surface and the heat shield fairing and in the region outside the heat shield fairing the grid is stretched exponentially.

3.5 Boundary conditions

Four distinct types of boundary conditions were used in the present analysis:

1. Inflow boundary
2. Outflow boundary
3. Symmetry boundary
4. Solid wall boundary

In the inflow boundary (AD), not only the velocity components but also the density and energy have to be prescribed. A typical treatment of the outflow boundary (DC) is either to specify the outflow velocities or set the velocity components equal to those located one vertex in. This generally works properly for high speed flow, but for low speed or incompressible flow, the prescription requires adjustment if it affects the upstream flows. In the present analysis we have used a specified pressure boundary. It uses fictitious cells for pressure definition. For a symmetry boundary condition (BC), the normal wall velocity must be kept zero throughout the calculation. If such a boundary is parallel to the x or y axis, the axial velocity is set to zero on a left or right boundary, or the radial component of velocity is set to zero on a bottom or top boundary. If the wall is slanted or curved, both the velocity components must be adjusted to make the flow tangential to the local slope. For the solid wall boundary (AB), the velocity components are set to zero regardless of wall orientation or curvature.

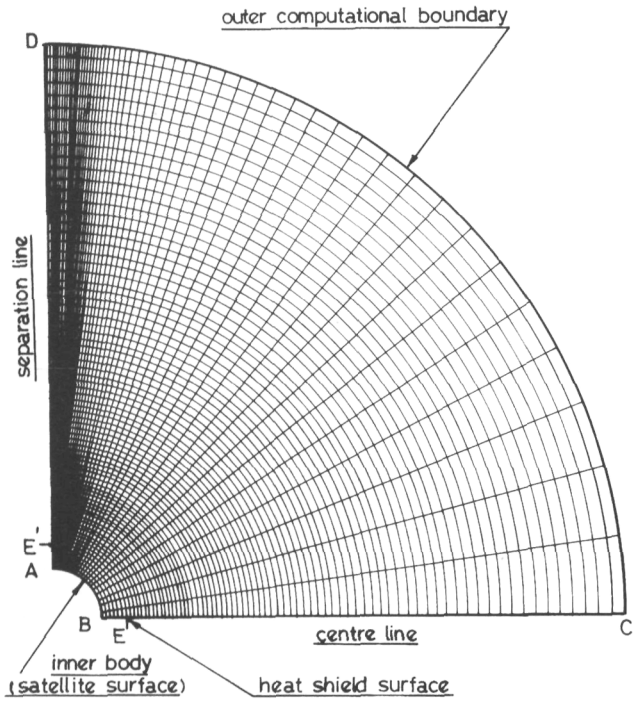

Figure 3. Computational grid.

4.0 RESULTS AND DISCUSSIONS

The validation of the software was done by comparing the computed results with the experimental results of the PSLV heat shield separation test on air. In the beginning a small gap of 5mm between the heat shield fairing and the plane of separation was provided to allow the flow inside and outside the compartment to interact. This initial gap is kept fixed until 5ms when the bellow loses contact with the heat shield fairing as observed in the experiment. Afterwards the new position of the fairing is calculated after every millisecond from the computed velocity and the grid is redefined for that new position of the heat shield fairing.

In order to estimate the variation of pressure drop at various locations inside the heat shield compartment, detailed measurements[4] were conducted. Figure 1 gives the location of the pressure sensors for the experiment. Two sensors (cp_3, cp_5) were provided for the outer surface of the heat shield fairing. Four sensors (cp_{10}, cp_9, cp_4, cp_2) to determine the longitudinal variation and another four sensors (cp_7, cp_6, cp_4, cp_8) were provided inside the compartment to determine the circumferential variations of temporal pressure behaviour. Two other sensors (cp_{11}, cp_{12}) were placed at the $R/2$ and $R/4$ location at the centre of gravity (CG) plane inside the heat shield compartment.

Figure 4 presents the comparison of measured and computed values of the transient delta pressure (kPa) (differential pressure from the atmospheric value) at the inner surface at the CG plane. Good overall agreement is observed between the two, except for the time of occurrence of the pressure recovery. The computed time of occurrence of the pressure recovery is about 10ms later than that of the

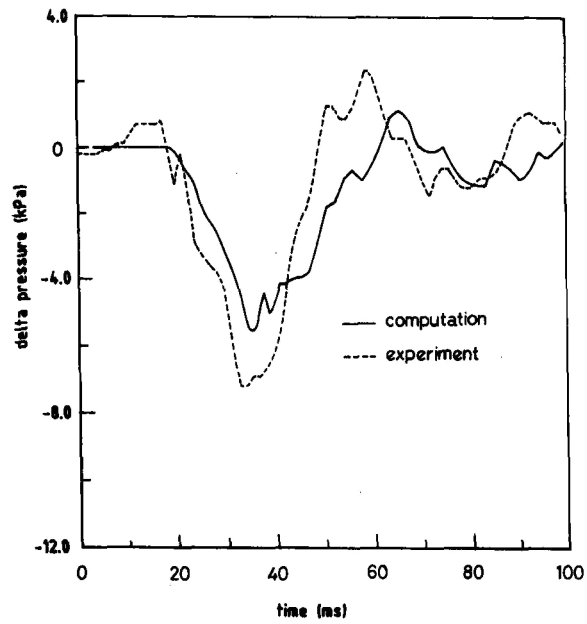

Figure 4. Pressure profile at inner surface at the CG plane.

experimental value. The initial overshoot present in the measured data during 10–20ms is due to experimental noise. As the command for ignition of explosive cord is given only at 19ms, no changes in the pressure are expected before that instant. The difference in the magnitude of the peak pressure drop between the measured and the predicted value is about 20%.

Figure 5 gives the transient pressure profile at the plane of symmetry on the outer surface of the heat shield fairing. Pressure at the outer surface keeps on increasing up to 5ms because of zip cord acceleration. After 5ms, when the fairing loses contact with the bellow, the pressure at the surface slowly comes down to atmospheric level. The small oscillation in the pressure in the later part is due to the reflection of the waves from the outer computational boundary and also due to numerical oscillation. Comparison with the experimental data shows a good overall agreement.

Figure 6 depicts the measured internal surface pressure drop at various circumferential locations. It is noted that at any particular instant of time, the circumferential variation of the surface pressure drop is almost negligible. This may be compared with the computed values of the circumferential variation of the pressure drop at the instant of 29·39 and 34·31 milliseconds given in Fig. 7.

Figure 8 shows the comparison of experimental and computed pressure drop at the inner surface and the $R/2$ location at the plane of symmetry. As expected on the inner surface the pressure drop starts from 19ms onwards, whereas at the $R/2$ location the pressure remains constant at the atmospheric level until the pressure waves reach the centrebody surface. The time matches well with the time the sound wave take to travel the distance of 0·8m (the distance between the centrebody surface and the heat shield fairing). This provides a check on the correctness of the calculation. The peak pressure drop and the overshoot for $R/2$ location is slightly more than that of the inner surface location. In the remaining part, the behaviour of the two curves is almost similar. The comparisons of the experimental data for the two locations also show a similar trend. The longitudinal variation of the internal pressure drop observed in the test is given in Fig. 9. As expected, the pressure drop at the top location (near the nose cap) is more than that at the bottom location. It may be recalled that the present computation cannot predict this longitudinal variation because the formulation assumes two-dimensionality.

Figure 10 gives the computed acceleration profile of the fairing. Up to 5ms, when the fairing is in contact with the zip cord bellow, the acceleration is mainly dominated by the zip cord acceleration. When the fairing loses contact with the bellow, it is subjected only to atmospheric drag which is caused by the pressure differential between inner and outer surfaces. Figure 11 presents the pressure profile at the plane of separation. The unsteady nature of the flow field appears truly physical, related to the vortex shedding from the edge of the fairing. As our interest is primarily related to the surface pressure on the heat shield, no attempt was made to capture the vortex motion in the computation. This unsteadiness is confined upto a few cells near the plane of separation. This is not found to influence the flow field in the plane of symmetry.

In order to analyse the effect of grid size, simulations were also carried out for another grid of size 50 × 46. Figure 12 compares the

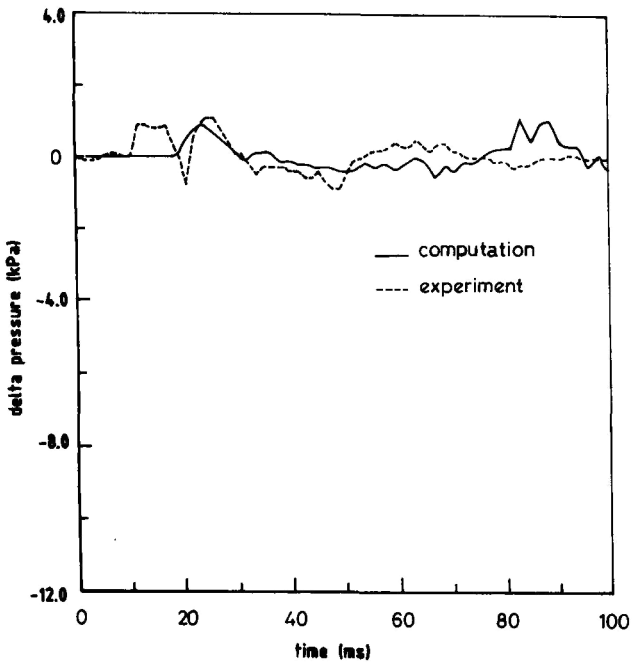

Figure 5. Pressure profile at outer surface.

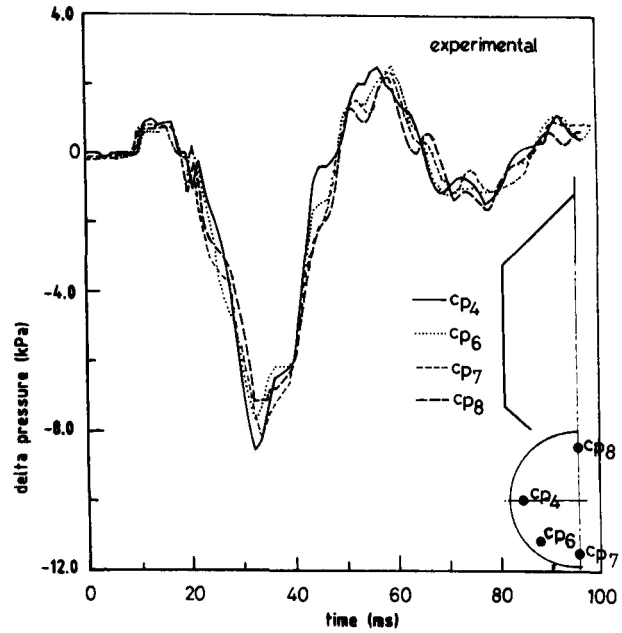

Figure 6. Circumferential variation of internal surface pressure drop (experimental).

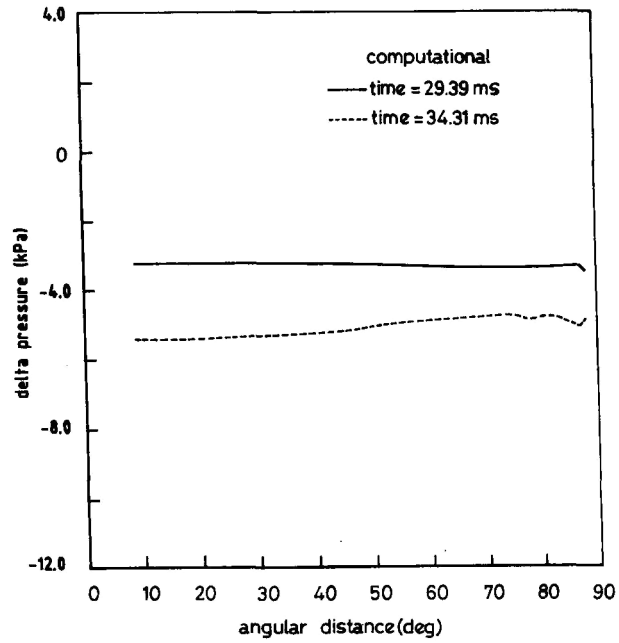

Figure 7. Circumferential variation of internal surface pressure drop (computational).

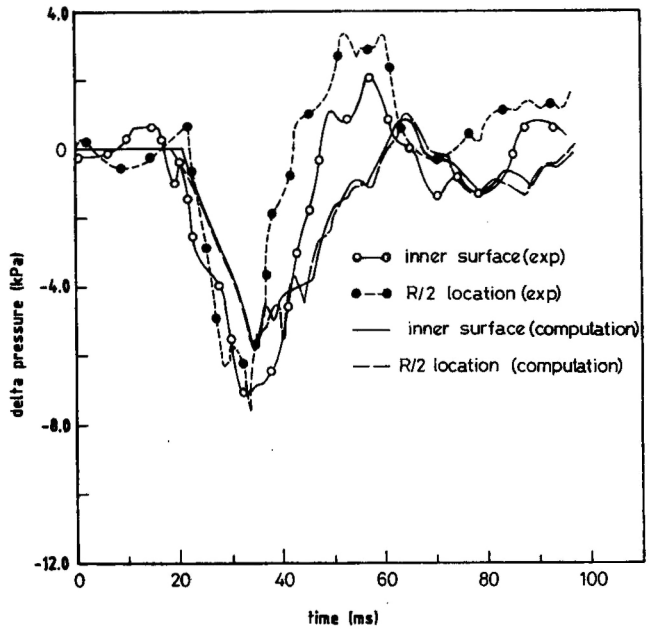

Figure 8. Radial variation of pressure drop.

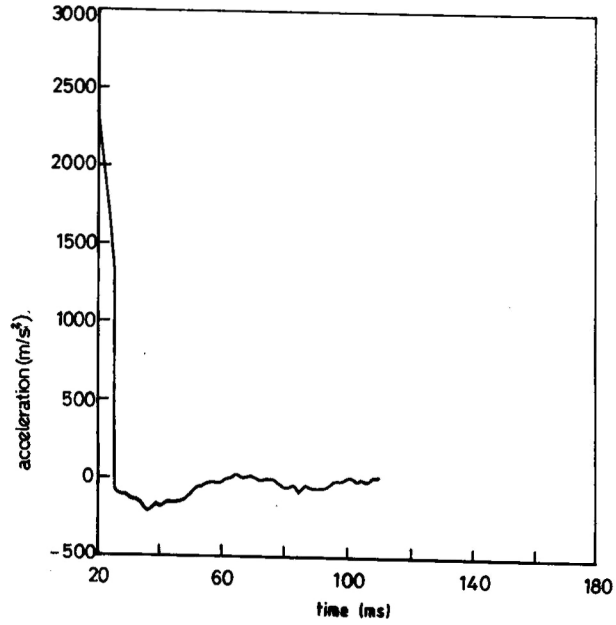

Figure 10. Acceleration profile.

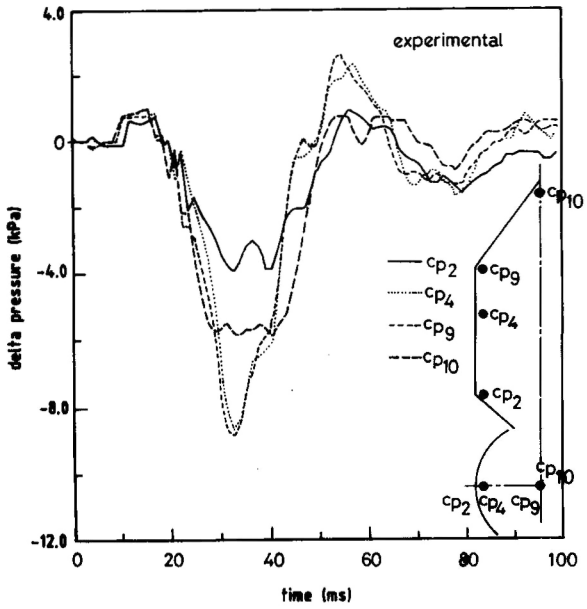

Figure 9. Longitudinal variation of internal surface pressure drop.

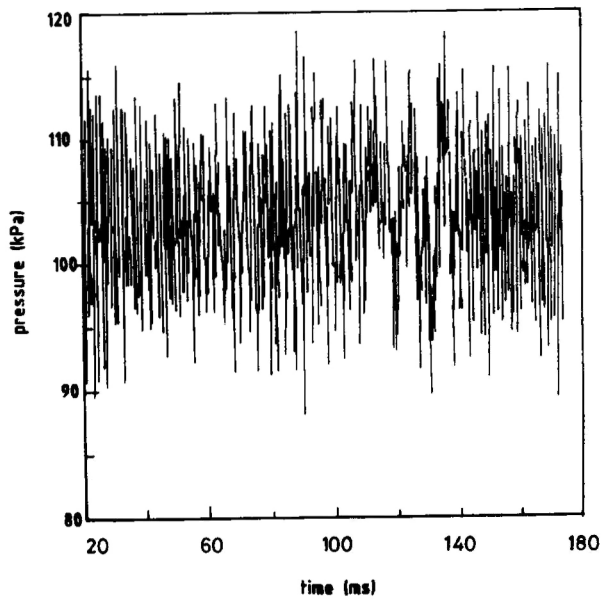

Figure 11. Pressure distribution on outer surface at the plane of separation.

compartmental pressure drop at the $R/2$ location for the two grids at the plane of symmetry, which clearly indicates the grid independence of the results.

In order to find out the effect of the initial gap between the plane of separation and the heat shield fairing in the solutions, computations were performed by taking the initial gap of 5mm, 15mm and 30mm. Transient pressure profiles at the $R/2$ location with different initial gaps are shown in Fig. 13. It has been found that with the increase in the gap the maximum pressure drop decreases. Moreover the overshoot, which is present for the gap of 5mm, is not noticed for the other two cases. Based on this observation, we can infer that for a proper simulation it is necessary to take the initial gap as small as possible.

For the stability of the scheme the following conditions on time step as suggested by Amsden *et al*[6] is observed throughout the computation:

- Courant condition on sound signal propagation is not violated.
- Fluid cannot move more than approximately one cell width per time step.
- For viscous effect, in every cell momentum must diffuse less than one cell width per time step.
- Time step should not increase more than 5% from the time step of the previous cycle.
- Time step should not be greater than the maximum time step for calculation (prescribed).

SALE algorithm is generally considered to be first order accurate[6]. A spectrum of computer runs with different mesh, time steps, artificial viscosity, convergence criteria, etc, were made to determine if a calculated effect is physical or simply a numerical artifice. Apart from this type of brute force approach, it has also been checked that

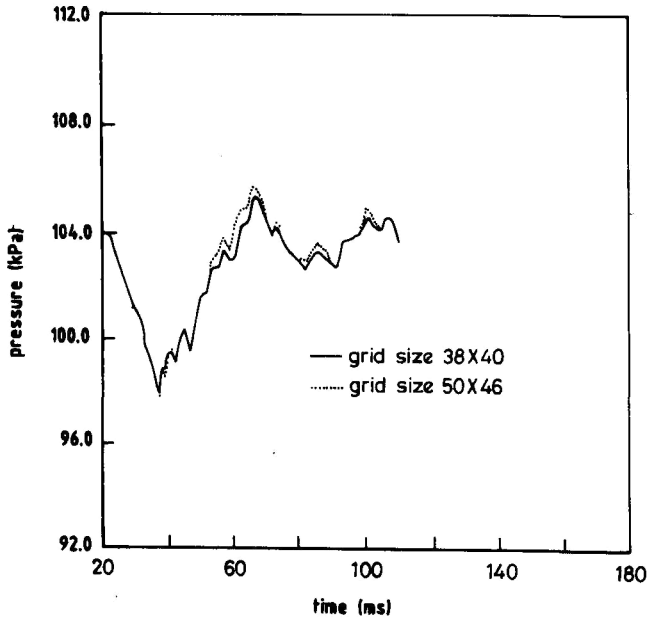

Figure 12. Pressure profile at $R/2$ location (grid independence result).

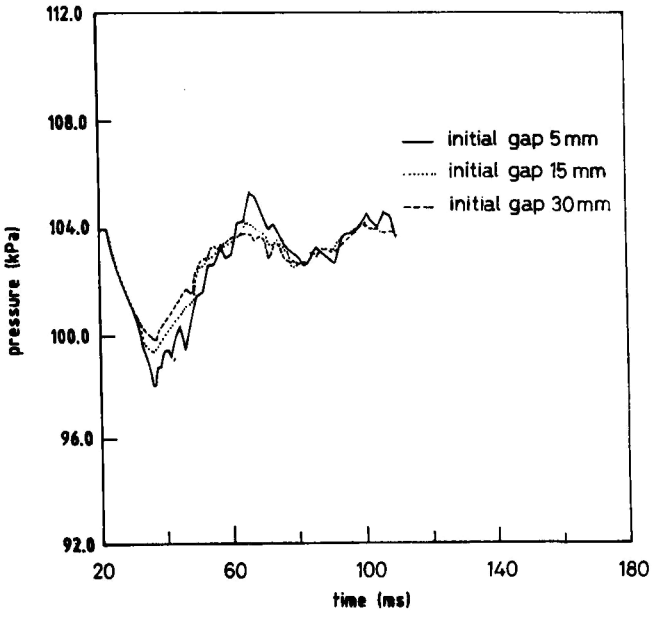

Figure 13. Pressure profile at $R/2$ location (effect of initial gap).

the solution does not exhibit large variations over distances comparable to cell width.

The simulations were carried out in the workstation based on Intel 860 chips. For a moderate grid of 38 × 40, the software take about 0·18 seconds per iteration. The total number of iterations required for calculating the flow field for 100ms is about 60,000.

5.0 CONCLUSIONS

To explain the phenomena of the compartmental pressure drop and to simulate the aerodynamics of the heat shield separation on the ground, software has been developed to solve the two-dimensional Navier-Stokes equations by using the Simplified Arbitrary Lagrangian Eulerian (SALE) numerical algorithm. The developed software was validated by comparing the computed results with the results of the full scale heat shield qualification test of the Indian Polar Satellite Launch Vehicle on the ground.

The prediction captures all essential features of the temporal behaviour of internal pressure including the time of occurrence of peak, overshoot, etc. The difference of the computed magnitude of the peak drop to that of experiment is about 20%. A good match has been observed between experiment and computation for the pressure profile at the outer surface of the heat shield fairing. The computed results indicated that the pressure at the $R/2$ location was not very different from that on the internal surface as observed in the experiment. No appreciable variation of internal pressure drop along the circumference has been observed in both experiment and computation. Understanding of aerodynamic process involved in the separation test in the air was found to be very helpful in extrapolating the test results to the flight conditions and a successful design of a heat shield separation system was made without a test in vacuum chamber, leading to a large cost savings.

It is necessary to extend the program for a three-dimensional case to capture all the behaviour of the internal pressure drop in the longitudinal direction inside the heat shield compartment. It may be noted that the edge effects will introduce a nose closing tendency during separation. The presence of such a tendency was confirmed by the test data. Time accuracy has also to be introduced to make it faster and more efficient numerically.

ACKNOWLEDGEMENT

The authors are grateful to Sri Abdul Majeed and Sri P.R.M. Panickar, ASMG, VSSC, for providing the experimental results for comparisons. The authors are thankful to Dr Rajeev Lochan and Dr V. Adimurthy, VSSC for their valuable suggestions.

REFERENCES

1. BUTCHER, J.R. The separation test in vacuum of the ARIANE 4 payload fairing, 15th space simulation conference, NASA-CP-3015, pp 372-391, 1988.
2. ROBINNS, M.J. Ground test program for new ATLAS payload fairings, Research in structures, structural dynamics and materials, NASA-CP-3064, pp 193-205, 1990.
3. YASUNGA, Y., FUKUSHIMA, Y., NAKAMURA, T. and FUJITA, T. Separation jettison test of Japanese H-II rocket satellite fairing, AIAA-90-0720, AIAA 28th Aerospace Science meeting, Reno, USA, January 8-11, 1990.
4. MADAVA PANICKER, P.R., RAMCHANDRAN, N. and POTTI, K.V.N. PSLV heat shield qualification test -02 results, VSSC-ASMG-TR-058/2, 1992.
5. HIRT, C.W., AMSDEN, A.A. and COOK, J.L. An arbitrary Lagrangian-Eulerian computing method for all speeds, *J Comp Phys*, 1974, **14**, (3), pp 227-253.
6. AMSDEN, A.A., RUPPEL, H.M. and HIRT, C.W. SALE: A simplified ALE computer program for fluid flow at all speeds, LA-8095, June 1980.